Guided propagation of surface acoustic waves in AlN and GaN films grown on 4*H*–SiC(0001) substrates

Y. Takagaki, P. V. Santos, E. Wiebicke, O. Brandt, H.-P. Schönherr, and K. H. Ploog
Paul-Drude-Institut für Festkörperelektronik, Hausvogteiplatz 5-7, 10117 Berlin, Germany
(Received 9 August 2002; published 31 October 2002)

The propagation modes of surface acoustic waves (SAW) in AlN and GaN layers are identified for the case of the acoustic wave being confined in the epitaxial layers by the fast-velocity SiC substrate. Higher-order Rayleigh modes emerge when the SAW wavelength is reduced to be below the layer thickness. We also report on the observation of an extremely-high-velocity SAW mode, which exists when the SAW wavelength is about an order of magnitude larger than the layer thickness. These guided modes enable us to utilize SAW velocities which can be even larger than the Rayleigh velocity in the substrate while maintaining the large electromechanical coupling coefficient of the overlayer.

DOI: 10.1103/PhysRevB.66.155439 PACS number(s): 68.35.Iv, 68.60.Bs

I. INTRODUCTION

In the last decade, epitaxially grown GaN and AlN layers have attracted a great deal of interest in optic and electronic applications. The large band gap of GaN has been successfully applied to realize light-emitting diodes and laser diodes in the blue and ultraviolet spectral range. The large band gap is useful also for high-power and high-temperature electronic devices. Furthermore, these materials possess high sound velocities and electromechanical coupling coefficients k^2_{eff}, making them suitable for high-frequency surface-acoustic-wave (SAW) filters,[1–3] which are a critical component in communication systems. These advantageous properties of GaN and AlN imply a potential for a new type of devices, in which the optic, electronic, and acoustic features are hybridized.[4,5]

At present, GaN and AlN films are typically grown on substrates like sapphire, SiC, and Si. To utilize the acoustic properties in these layered structures, one has to take into account the velocity mismatch between the overlayer and the substrate. Various SAW modes are anticipated to appear in addition to the ordinary Rayleigh mode.[6,7] The most important parameter that governs the emergence of these SAW modes is the ratio between the SAW wavelength λ_{SAW} and the film thickness d. For $\lambda_{\mathrm{SAW}} > d$, the influence of the layered nature is, in principle, to modify the SAW velocity. On the contrary, the interference effect arising from the reflection of the acoustic waves from the substrate becomes important when $\lambda_{\mathrm{SAW}} < d$. The everlasting demand to raise the operation frequency of the SAW devices urges the reduction of λ_{SAW}. Therefore, the role of the velocity mismatch becomes inevitably important in high-frequency SAW devices.

In this paper, we investigate the SAW transmission properties in GaN/SiC and AlN/SiC heterostructures. The SAW velocity in SiC (6832 m/s) is larger than the velocities in GaN (3693 m/s) and AlN (5790 m/s). The acoustic waves are hence confined in the slow-velocity films. The guiding of the SAWs gives rise to the appearance of higher-order Rayleigh modes. The variation of the velocities associated with these SAW modes when λ_{SAW}/d is changed will be compared with the prediction by theory. We will also discuss a SAW mode that propagates nearly twice as fast as the Rayleigh modes.

II. EXPERIMENT

The GaN and AlN films were grown on semi-insulating 4H–SiC(0001) substrates (this polytype of SiC is hexagonal and has four layers per unit cell) by plasma-assisted molecular-beam epitaxy. The substrate temperature was 800°C. The plasma power of 180 W (300 W) and the N_2 flow of 1 sccm yielded a N-limited growth rate of 0.25 μm/h (0.5 μm/h) for the AlN (GaN) films. Growth was monitored *in situ* by reflection high-energy electron diffraction (RHEED). The effective surface stoichiometry was adjusted to be as close to unity as possible, exploiting the recovery of the RHEED intensity upon growth interruptions.[8] As a result, the AlN (GaN) films feature smooth surfaces with typical values for the peak-to-valley roughness of 5–15 nm (3–10 nm) and for the rms roughness of 0.5–2 nm (0.3–1 nm) over an area of 2×2 μm^2. The width of the (0002) x-ray rocking curve as measured by double crystal x-ray diffractometry amounts to 200–400″ for the AlN films and 100–200″ for the GaN films. We list in Table I the samples that we employed in our experiment. All the AlN layers were highly-

TABLE I. Thickness of the layers for the AlN/SiC and GaN/SiC structures and carrier density for the GaN layers at room temperature. The delay lines were fabricated in the *C*-plane along the crystallographic directions indicated.

	Structure	Thickness (μm)	Carrier density (10^{24} m^{-3})	SAW direction
A1	AlN/SiC	0.25	···	$[1\bar{1}00]$
A2	AlN/SiC	0.5	···	$[1\bar{1}00]$
A3	AlN/SiC	1.0	···	$[1\bar{1}00]$
A4	AlN/SiC	1.25	···	$[1\bar{1}00]$
G1	GaN/SiC	0.7	0.9	$[11\bar{2}0]$
G2	GaN/SiC	0.95	4.2	$[11\bar{2}0]$
G3	GaN/SiC	1.5	0.05	$[1\bar{1}00]$

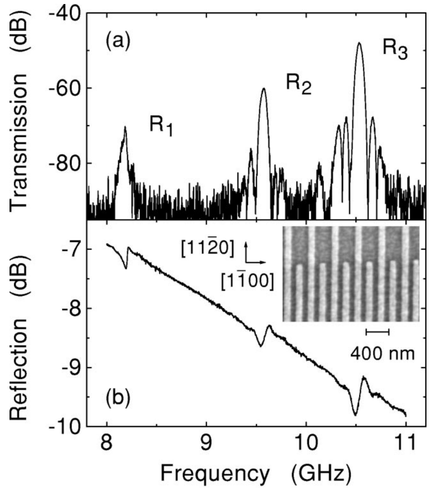

FIG. 1. (a) Transmission and (b) reflection characteristics of a delay line having the SAW wavelength $\lambda_{SAW}=0.7$ μm prepared on the AlN/SiC structure with thickness $d=1.25$ μm. The resonances labeled R_1, R_2, and R_3 are associated with the first-, second-, and third-order Rayleigh modes, respectively. Inset: Scanning-electron-microscope image of a single-finger IDT having a transducer period of $\lambda_{SAW}=$ 400 nm fabricated on the AlN/SiC structure. The SAWs are generated in the $[1\bar{1}00]$ crystallographic direction.

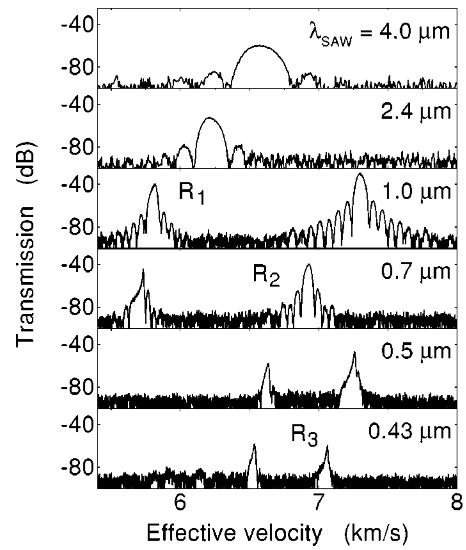

FIG. 2. Dependence of the SAW transmission on the wavelength λ_{SAW} in the AlN/SiC structure with the film thickness $d=1$ μm. The number of finger pairs is 25, 41.5, 100, 114, 160, and 160 for $\lambda_{SAW}=$ 4.0, 2.4, 1.0, 0.7, 0.5, and 0.43 μm, respectively.

resistive. In contrast, the GaN layers G1 and G2 were intentionally doped, while sample G3 exhibited a background electron density of 5×10^{16} cm^{-3}.

We fabricated single-finger interdigital transducers (IDTs) on the epitaxial layers by means of electron-beam lithography and lift-off techniques. The inset of Fig. 1(b) shows the scanning-electron-microscope image of one of the transducers. Here, the SAW wavelength, which is twice the period of the grating pattern, is $\lambda_{SAW}=400$ nm. The metal gates of the IDTs are made of a 25-nm-thick evaporated Al film. A 6-nm-thick Ti film was inserted underneath the Al film to improve the adhesion of the gates to the epitaxial layers. By aligning two identical transducers, SAW delay lines were formed with a center-to-center separation of 0.5 mm. As the SAW propagation is expected to be isotropic in the C-plane of the hexagonal crystals, we stretched the delay lines along the cleavage directions of the crystals. In most of our devices, the SAWs were made to propagate along the $[1\bar{1}00]$ crystallographic direction, see Table I.

The transmission and reflection characteristics of the delay lines were evaluated using an HP 8720D network analyzer. The impulse response of a delay line can be obtained by Fourier-transforming its transmission spectrum. The direct electromagnetic coupling between the transducers takes place much faster than the SAW propagation, so that the crosstalk can be isolated from the SAW transmission spectrum by filtering the corresponding component in the time domain. This gating technique has been applied for the transmission data to be presented below.

III. EXPERIMENTAL RESULTS

Figures 1(a) and 1(b) show, respectively, the transmission and reflection amplitudes in a delay line having $\lambda_{SAW}=0.7$ μm, which was defined on a 1.25-μm-thick AlN film (sample A4). Both of the spectra exhibit three clear resonances. The resonance at 8.19 GHz, labeled R_1, is associated with the first-order Rayleigh mode, which is the normal SAW mode in piezoelectric materials. As λ_{SAW} is considerably less than d, the resonances associated with the second- (R_2) and third-order (R_3) Rayleigh modes are, at the same time, observed at 9.58 and 10.53 GHz, respectively. The SAW velocity increases with increasing the order of the Rayleigh mode. Consequently, a higher-order mode results in a resonance at a higher frequency.

The behavior of the SAW transmission properties when λ_{SAW} is varied between 4.0 μm and 0.43 μm is shown in Fig. 2. Here, the delay lines were fabricated on an AlN film with $d=1$ μm (sample A3). The SAW transmission is solely mediated by the first-order Rayleigh mode for the fundamental frequency of the IDTs when $\lambda_{SAW}=4.0$ and 2.4 μm. Upon reducing λ_{SAW}, the second- and third-order Rayleigh modes emerge when λ_{SAW} is smaller than 1.0 and 0.5 μm, respectively. The higher-order Rayleigh modes can be regarded as higher-order "transverse modes" in the AlN waveguides. Analogous to the waveguide modes, the ith-order Rayleigh mode appears when the ratio d/λ_{SAW} is larger than approximately $i-1$. We note that SAWs propagate slower in sapphire than in AlN. Therefore, the guided modes are not expected to appear for AlN layers grown on sapphire.

The symbols in Fig. 3 show the SAW velocity determined using the resonance frequency and λ_{SAW}. We emphasize that the data from all of the four AlN layers exhibit a universal behavior when λ_{SAW} is normalized by d. We observe up to the fourth-order Rayleigh mode in our devices. The SAWs localize at the immediate vicinity of the surface over a distance of about one wavelength. Thus, the SAW velocities decrease with reducing λ_{SAW} due to the progressive influence of the slow-velocity AlN overlayer. The variation of the

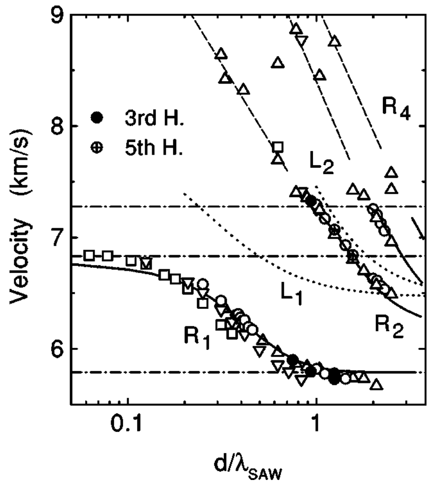

FIG. 3. Dependence of the SAW velocities on the normalized inverse SAW wavelength d/λ_{SAW} in AlN/SiC structures. The thicknesses of the AlN films are 0.25 (squares), 0.5 (down triangles), 1.0 (circles), and 1.25 μm (up triangles). The data from the third and fifth harmonics are included for the 1.0-μm-thick film. The solid lines show theoretical results for the Rayleigh modes R_i. The dashed lines are guides for the eyes. The velocity predicted for the lowest two Love modes L_i are shown by the dotted lines. The dashed–dotted lines indicate the velocities of the bulk transverse wave in SiC and the Rayleigh waves in SiC and in AlN from the top to the bottom, respectively.

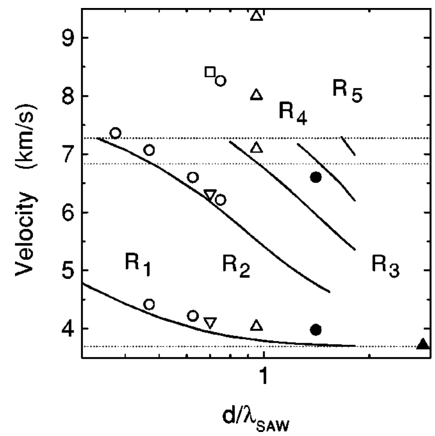

FIG. 4. Dependence of the SAW velocities on the normalized inverse SAW wavelength d/λ_{SAW} in GaN/SiC structures. The thicknesses of the GaN films are 0.7 (down triangles), 0.95 (up triangles), and 1.5 μm (circles). The filled symbols indicate the third harmonic. The solid curves show theoretical results. The dotted lines indicate the velocity of the bulk transverse wave in SiC and the SAW velocities in SiC and in GaN from the top to the bottom, respectively.

depth profiles of the displacement fields is responsible for the SAW velocity of the first-order Rayleigh mode shifting from that of the substrate to that of the overlayer when $d/\lambda_{SAW} \to \infty$. In striking contrast to this dispersion, the SAW velocities associated with the higher-order Rayleigh modes can be even faster than the SAW velocity in the SiC substrate. The higher-order Rayleigh modes are, hence, advantageous for high-frequency SAW devices.

Figure 3 contains also the data derived from the third and fifth harmonics. It should be noted that the harmonics were excited unexpectedly strongly in spite of the single-finger gates of the devices. The harmonics were observed when λ_{SAW} of the fundamental frequency was longer than ≈ 2 μm. In principle, the inability of exciting the harmonics for $\lambda_{SAW} < 2$ μm could result from the impedance mismatch between the measurement equipment and the IDTs. (The impedance of ITDs is determined by the aperture, which was 50–100 μm in our devices.) Nevertheless, the long SAW wavelengths, i.e., $\lambda_{SAW} > d$, suggest that the layered nature of the structure plays an important role for the remarkable efficiency to excite the harmonics. Owing to the large λ_{SAW} in this situation, a single peak was observed for the fundamental frequency, whereas multiple peaks resulting from additional higher-order Rayleigh modes were typically observed for the harmonics.

Similar results for GaN/SiC structures are presented in Fig. 4. Five branches associated with the Rayleigh modes R_1–R_5 are evident. The electromechanical coupling coefficient of GaN is smaller than that of AlN. The transmission amplitude in devices prepared on GaN was consequently smaller in comparison to that when the overlayers were AlN. Nevertheless, the range of the velocity modification is more than two times wider in GaN/SiC structures than in AlN/SiC structures due to the comparatively small SAW velocity in GaN, which may be useful from an application point of view.

Although the SAW velocities are determined solely by the ratio d/λ_{SAW}, we observe a crucial dependence of the transmission amplitude on the layer thickness. In Fig. 2, a lower-order Rayleigh mode disappears the moment a higher-order mode emerges with decreasing λ_{SAW}. Only two peaks, as a consequence, coexist in the transmission spectra. In thicker films, however, more resonances can coexist. For instance, three peaks are seen in the transmission spectrum displayed in Fig. 1, for which $d = 1.25$ μm instead of $d = 1.0$ μm in Fig. 2. Likewise, thinner films can sustain fewer resonances simultaneously. This trend develops to such an extent that the transmission amplitude associated with the first-order Rayleigh mode was suppressed for $d = 0.25$ μm below the detection limit (~ -100 dB) when λ_{SAW} was smaller than 700 nm, whereas the second-order Rayleigh mode became strong enough for detection only when λ_{SAW} was less than 500 nm (not shown). No SAW transmission was, therefore, observed for 700 nm $> \lambda_{SAW} >$ 400 nm. A possible explanation for this behavior is the small electromechanical coupling coefficient of SiC. The coupling coefficient of SiC is estimated to be one order of magnitude smaller than that of AlN (see the Appendix). Thus, the SAW excitation is expected to become difficult when the thickness of the top AlN layer is reduced. We note that the first-order Rayleigh mode seemed to disappear for $\lambda_{SAW} <$ 0.7 μm irrespective of *d*. The common critical SAW wavelength suggests that intrinsic properties of the epitaxial layers may be responsible for the disappearance.

IV. NUMERICAL RESULTS

We have carried out numerical simulations of the SAW modes in the AlN/SiC and GaN/SiC structures for under-

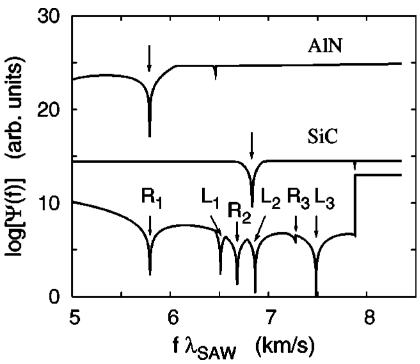

FIG. 5. Boundary-condition function $\Psi(f)$ in AlN, SiC, and the AlN/SiC structure with an overlayer thickness of 1.25 μm for the curves from top to bottom. The curves are vertically offset for clarity. The calculations were performed for a SAW with wavelength $\lambda_{SAW}=0.7$ μm. R_i and L_i denote Rayleigh- and Love-type modes of order i, respectively.

standing their nature. The surface of bulk hexagonal materials normally supports only one acoustic mode. This property is demonstrated by the top two curves in Fig. 5. Here, the dependence of the boundary-condition function $\Psi(f)$ on frequency f is displayed for AlN and SiC. (See the Appendix for details of the numerical techniques.) The calculations were performed for $\lambda_{SAW}=700$ nm. A surface mode corresponds to a frequency f_R where $\Psi(f)$ vanishes, as indicated by the arrows, giving rise to the Rayleigh velocity $v_R=f_R\lambda_{SAW}$.

In layered structures, in contrast, $\Psi(f)$ develops multiple minima. The bottom curve in Fig. 5 displays $\Psi(f)$ for the 1.25-μm-thick AlN film on SiC (sample A4). Except for the mode labeled R_3, $\Psi(f)$ vanishes at the frequencies indicated by the arrows. Here, the modes polarized in the sagittal plane are denoted by R_i ($i=1,2,\ldots$). The mode R_1 closely resembles the Rayleigh wave in the surface of bulk AlN, as we show below. The rest of the surface modes in Fig. 5(c), which are denoted by L_i, are pure shear vibrations polarized in the surface perpendicular to the propagation direction (Love-type modes). Love modes are characteristic vibrations of substrates covered by a low-velocity film.[6,9] The present acoustic waveguide supports, in addition to the fundamental mode L_1, two overtones (L_2 and L_3) having the velocities between those of the fast transverse bulk modes of AlN and SiC.

Provided that the mass-loading effects due to the metal gratings are negligible,[10] the velocities of the surface modes in the layered structures depend only on the ratio d/λ_{SAW}. In Figs. 3 and 4, the calculated velocities of the Rayleigh-type (solid curves) modes are shown for the AlN/SiC and GaN/SiC structures, respectively. For comparison, we also show the velocities of the lowest two Love-type modes (dotted curves) in Fig. 3. The Rayleigh-type modes indeed account for the measured resonances. The Love-type modes are piezoelectrically inactive in the AlN/SiC and GaN/SiC structures, which is the reason for their absence in the electrical measurements. Such modes, however, have been detected in Brillouin scattering experiments in GaN and AlN overlayers on silicon.[11]

In Fig. 6, we illustrate the vertical displacement u_3 for the three Rayleigh modes revealed by the bottom curve in Fig. 5. Mode R_1 [Fig. 6(a)] has a penetration depth which is shorter than the thickness of the AlN layer and closely resembles the Rayleigh wave in bulk materials. Modes R_2 [Fig. 6(b)] and R_3 [Fig. 6(c)] are overtones of the fundamental Rayleigh mode R_1. The overtones are characterized by nodes in the depth-direction.[6,11] The number of nodes increases for higher-order modes, reminiscent of the confined modes in waveguides.

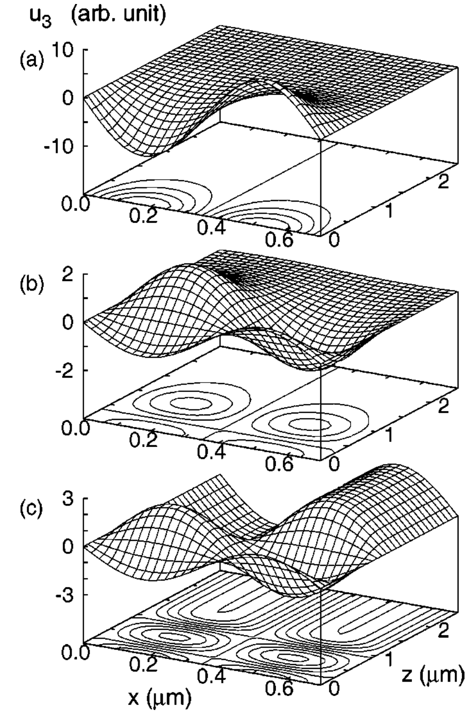

FIG. 6. Calculated vertical displacement (u_3) profiles for modes (a) R_1, (b) R_2, and (c) R_3 with wavelength $\lambda_{SAW}=0.7$ μm in a structure consisting of a 1.25-μm-thick AlN layer on SiC.

Modes R_1 and R_2 are true surface modes as their velocities lie below those of the longitudinal bulk mode v_L and the slow transverse bulk mode v_{T_1} of the SiC substrate. Mode R_3, on the contrary, is a leaky mode as its velocity is above v_{T_1}. In fact, an upper limit is imposed theoretically upon the velocities of the surface modes by v_{T_1} of the substrate. Whenever the ith-order Rayleigh mode emerges at $d/\lambda_{SAW}=i-1$, its velocity takes a common initial value v_{T_1}. As v_{T_1} is higher than the Rayleigh velocity, the higher-order modes R_i ($i>1$) can propagate even faster than the Rayleigh mode in bulk SiC.

Experimentally, some of the data indicate velocities which are considerably larger than v_{T_1}. Such a situation is, in principle, possible for short delay lines if the transmission loss associated with the leaky nature of the SAW modes is not critical. Nevertheless, the experimental results suggest that v_{T_1} in SiC may be larger than our estimate. The latter implies that the elastic constant c_{44} is larger than the value we used in our calculations as $v_{T_1}=\sqrt{c_{44}/\rho}$, with ρ being the mass density, is practically determined by c_{44}. In fact, our value of c_{44} has been chosen to achieve the best agreement with the

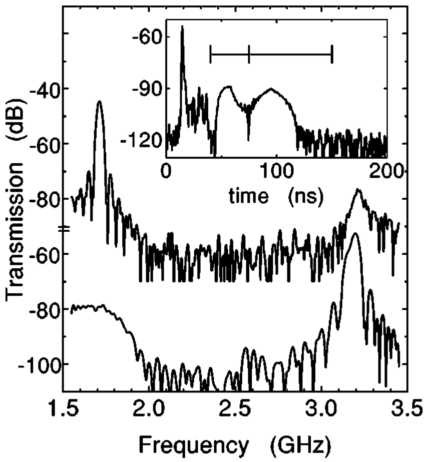

FIG. 7. Transmission spectra of a delay line prepared on the AlN/SiC structure. The film thickness and the SAW wavelength are $d=$ 250 nm and $\lambda_{SAW}=4.0$ μm. A gate window in the time domain with the interval of 40–75 ns and 75–150 ns is imposed for the top and bottom curves, respectively. Inset: The impulse response of the delay line produced by Fourier-transforming the transmission spectrum. The gate windows to isolate the two SAW modes are indicated. The peak at 14 ns is due to direct electromagnetic coupling between the IDTs.

experimental results and is already larger than found in the literature (see Ref. 8 in Ref. 12.)

V. EXCEPTIONALLY FAST MODE

In addition to the Rayleigh modes discussed above, some delay lines exhibited a resonance at a frequency significantly higher than that for the Rayleigh modes. An example of these unidentified resonances is shown in Fig. 7. Here, a delay line having $\lambda_{SAW}=4.0$ μm was fabricated on a 0.25-μm-thick AlN layer (sample A1). Two resonances are found at 1.712 and 3.197 GHz. The resonance at the lower frequency is associated with the first-order Rayleigh mode. The resonance frequency implies that the velocity of the mode at the higher frequency is about two times larger than that of the Rayleigh modes. The impulse response of the delay line, which is displayed in the inset of Fig. 7, indeed reveals two peaks that correspond to the fast and slow SAW modes. Using the gating technique, we can prove the assignment of the two modes. The two spectra in Fig. 7 were actually obtained by setting a window between 40 and 75 ns or between 75 and 150 ns: The low- (high-) frequency peak is absent when the fast- (slow-) propagation peak in the time domain is selected.

The high-velocity mode was found to be excitable only in a very narrow wavelength range. This behavior is illustrated in Fig. 8 for the case of the 1-μm-thick AlN layer (sample A3). For this layer thickness, the high-velocity mode is observed when λ_{SAW} is about 2.4 μm. In Fig. 8, λ_{SAW} is varied between 2.67 and 2.18 μm. With decreasing λ_{SAW}, both of the transmission peaks shift to higher frequencies. In contrast to the almost uniform peak amplitudes for the Rayleigh mode at $\sim$2.5 GHz, the high-velocity peak at 5–6 GHz develops and then vanishes quickly in the course of the slight variation of λ_{SAW}.

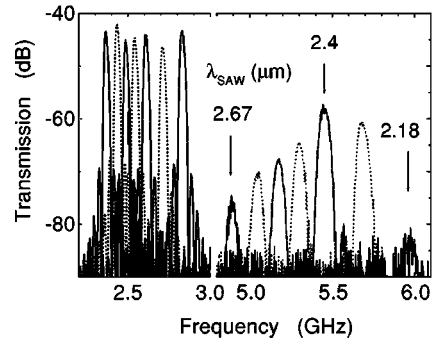

FIG. 8. Transmission spectra of delay lines fabricated on the 1-μm-thick AlN layer grown on a SiC substrate. The SAW wavelengths are $\lambda_{SAW}=$ 2.67, 2.59, 2.53, 2.46, 2.4, 2.29, and 2.18 μm.

The fast propagation may be attributed to the "exceptional" mode, which has been predicted to exist in some layered systems.[13–15] Leaky SAWs are typically strongly attenuated as the acoustic energy leaks into the bulk of the crystal. However, the attenuation vanishes when the leaky SAW degenerates into a pure bulk wave.[13] The velocity of the nonattenuated leaky SAW under this special circumstance was calculated for a ZnO film prepared on SiC,[14] diamond,[15] or sapphire[15] substrates. The SAW velocity was shown to change from the velocity of the longitudinal bulk wave v_L to that of the fast transverse bulk wave v_{T_2} of the substrate when d/λ_{SAW} is increased from 0 to about 0.1.

In Fig. 9, we make a comparison of the d/λ_{SAW}-dependencies of the velocity between the high-velocity mode and the guided Rayleigh modes in AlN/SiC structures. The data from $d=0.25$ and 0.5 μm layers appear to belong to an identical dispersion curve, whereas the data from $d=1.0$ μm layer apparently follow a different dispersion curve. It is thus indicated that two branches of the high-velocity mode have been observed in our devices. Although the velocity decreases with increasing d/λ_{SAW} for both of the branches, it remains almost around v_L, which is not ex-

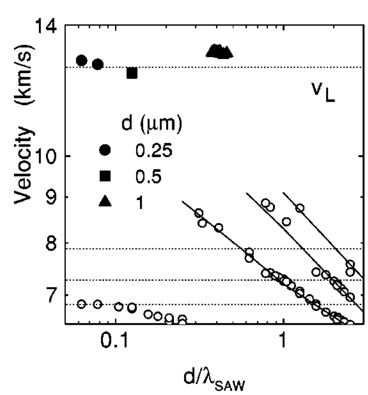

FIG. 9. Velocities of SAW modes in the AlN/SiC structures with several AlN layer thicknesses d. The open and filled symbols correspond to the Rayleigh modes and the exceptional high-velocity mode, respectively. The dotted lines indicate the velocities in SiC of the longitudinal bulk wave (v_L), the fast and slow transverse bulk waves, and the Rayleigh wave from top to bottom, respectively. The solid lines are guides for eyes.

pected for the "exceptional" mode. Further experimental and theoretical works are, therefore, required to ascertain the origin of this mode. We emphasize that, regardless of the origin, the high-velocity mode provides us nearly the largest possible sound velocity from host materials as v_L in SiC is as large as the Rayleigh velocity in diamond.

VI. CONCLUSIONS

We have investigated the SAW modes in AlN and GaN layers grown on SiC substrates. The slow SAW velocity of the top layers with respect to that of the substrate results in the appearance of guided Rayleigh modes and extremely fast modes. While the velocities associated with the SAW modes are determined solely by the ratio between the SAW wavelength and the layer thickness, the transmission amplitude of each mode is found to depend crucially on the layer thickness. As long as the layer thickness is adjusted to be optimum for the desired SAW wavelengths, the present materials systems allow us to take advantage of the high SAW velocity of SiC and the large electromechanical coupling coefficient of AlN and GaN.

ACKNOWLEDGMENTS

Part of this work was supported by the Deutsche Forschungsgemeinschaft and by the NEDO collaboration program.

APPENDIX. NUMERICAL SIMULATIONS

We present in this Appendix a brief overview of the numerical techniques that we employed in our calculations. The acoustic waves are assumed to propagate along the *x*-direction within a surface which is normal to the *z*-axis. The components u_1, u_2, and u_3 of the displacement field $\mathbf{u} = (u_1, u_2, u_3)$ are oriented along the *x*-, *y*-, and *z*-directions, respectively. The SAW modes in layered structures can be determined by solving the differential equation for the propagation of acoustic waves[16]

$$\nabla T = \rho \frac{\partial \mathbf{u}}{\partial t} \tag{A1}$$

together with the constitutive relations

$$T = cS - eE, \tag{A2}$$

$$D = \epsilon E + eS, \tag{A3}$$

where T and S are the stress and strain tensors, respectively. The electric and displacement fields are denoted $E = -\nabla \varphi$ and D, respectively. The material parameters involved in Eqs. (A1)–(A3) are the mass density ρ, the elastic constant tensor c, and the piezoelectric and static dielectric tensors e and ϵ, respectively. We list the values of these parameters used in the calculations in Table II.

In order to calculate the SAW modes, we first determine for each layer the solutions of Eq. (A1) for a frequency f and an in-plane wave vector $\mathbf{k}_{\mathrm{SAW}} = (k_x, k_y)$. These solutions consist of eigenvalues of the *z*-component of the wave vector k_z and the mode eigenvectors $\mathbf{v} = (u_1, u_2, u_3, \varphi)$. In the second step, the eigenvectors $\mathbf{v}$ in adjacent layers are related to each other by imposing acoustic and electric boundary conditions at their interface. This procedure allows us to specify the eigenvectors of the surface layer in terms of those in the substrate. In the final step, we seek for surface modes, i.e., the solutions which (i) decay in the substrate and (ii) satisfy the acoustic and electric boundary conditions at the surface. These requirements can be expressed in terms of the boundary-condition function $\Psi(f)$, which vanishes when both conditions are satisfied. The corresponding frequency f_R is the SAW frequency of the system.

In the remainder, we discuss the acoustic modes propagating in the hexagonal crystals of bulk AlN, GaN, and 4H-SiC. The velocities of the bulk modes are summarized in Table III. The acoustic velocities are isotropic for propagation in the *C*-plane. The modes with wave vector along the *x*-axis can be classified according to the symmetry relative to the

TABLE II. Mass density ρ, elastic constants c_{ij} (in units of 10^{11} N/m^2), and piezoelectric constants e_{ij} (in units of C/m^2) used in the calculations. All the constants for AlN and GaN are taken from Ref. 2. The elastic constants for SiC with the exception of c_{44} and c_{13} are from Ref. 12. [There is only a minor difference, mostly within the experimental accuracy, between the elastic properties of the 4H– and 6H–SiC polytypes (Ref. 12).] We use a value for c_{44} that better reproduces the transverse velocity of SiC. For c_{13}, which is not quoted in Ref. 12, we use the value recommended in Ref. 17. The piezoelectric constants are extracted from Ref. 18.

	AlN	GaN	4H-SiC
ρ (10^3 kg/m^3)	3.23	6.15	3.211
c_{11}	4.1	3.7	5.07
c_{12}	1.4	1.45	1.08
c_{13}	1	1.1	0.558
c_{33}	3.9	3.9	5.47
c_{44}	1.2	0.9	1.7
c_{66}	1.35	1.125	1.995
e_{15}	−0.48	−0.3	0.08
e_{31}	−0.58	−0.36	
e_{33}	1.55	1	0.2

TABLE III. Velocities of bulk (v_{T_1}, v_{T_2}, and v_L) and surface (v_R) modes and electromechanical coupling coefficient k^2_{eff} on *c*-oriented AlN, GaN, and SiC. Similar values are given also for sapphire $[1\bar{1}00]$-propagation, Y-cut $LiNbO_3$ Z-propagation, and (001)-oriented GaAs.

	v_{T_1} (m/s)	v_{T_2} (m/s)	v_L (m/s)	v_R (m/s)	k^2_{eff} (in 10^{-3})
GaN	3826	4277	7757	3693	1.31
AlN	6095	6465	11267	5790	2.5
4H–SiC	7276	7882	12566	6832	0.112
sapphire				5703	
$LiNbO_3$				3488	23.2
GaAs				2867	0.593

(x,y)-plane, which is a mirror plane for the layered structure. The longitudinal (L) and the slow transverse (T_1) modes have even symmetry with respect to the mirror plane. They are polarized in the sagittal plane, i.e., along the x- and y-directions for the L and T_1 modes, respectively. Their velocities are given by $v_L=\sqrt{c_{11}/\rho}$ and $v_{T_1}=\sqrt{c_{44}/\rho}$. The fast transverse mode T_2 is uneven. Its polarization is in the plane of the surface, i.e., perpendicular to the c-axis, and the velocity is given by $v_{T_2}=\sqrt{(c_{11}-c_{12})/(2\rho)}$.

Table III also lists the velocity v_R of surface modes in the bulk materials. These Rayleigh modes have polarization in the sagittal plane and, thus, their symmetry is even with respect to the mirror operation. The Rayleigh velocities in these hexagonal crystals are lower than those of the transverse bulk vibrations (this is not the case, for instance, for piezoelectric SAWs along the [110] direction in III–V compounds). These modes, therefore, cannot be easily scattered into bulk modes.

The last column of Table III lists the effective electromechanical coupling coefficient k^2_{eff} for the surface modes. Here, we adopt the definition of k^2_{eff} being twice the relative change in the SAW velocity when the surface is metallized.[9] The coupling coefficient for AlN is approximately twice as large as that of GaN. Although the coupling coefficients of AlN and GaN are larger than k^2_{eff} of GaAs, they are an order of magnitude smaller than k^2_{eff} of $LiNbO_3$, which is one of the most strongly coupling piezoelectric materials. We point out that SiC is very weakly piezoelectric. Therefore, bulk SiC is not promising for SAW devices in spite of the large SAW velocity.

[1] H. Okano, N. Tanaka, Y. Takahashi, T. Tanaka, K. Shibata, and S. Nakano, Appl. Phys. Lett. **64**, 166 (1994).
[2] C. Deger, E. Born, H. Angerer, O. Ambacher, M. Stutzmann, J. Hornsteiner, E. Riha, and G. Fischerauer, Appl. Phys. Lett. **72**, 2400 (1998).
[3] A. Khan, R. Rimeika, D. Čiplys, R. Gaska, and M. S. Shur, Phys. Status Solidi B **216**, 477 (1999).
[4] R. Rimeika, D. Ciplys, R. Gaska, J. W. Yang, M. A. Khan, M. S. Shur, and E. Towe, Appl. Phys. Lett. **77**, 480 (2000).
[5] P. V. Santos, J. Appl. Phys. **89**, 5060 (2001).
[6] E. H. El Boudouti, B. Djafari-Rouhani, and A. Akjouj, Phys. Rev. B **55**, 4442 (1997).
[7] X. Zhang, J. D. Comins, A. G. Every, P. R. Stoddart, W. Pang, and T. E. Derry, Phys. Rev. B **58**, 13 677 (1998).
[8] O. Brandt, R. Muralidharan, P. Waltereit, A. Thamm, A. Trampert, H. von Kiedrowski, and K. H. Ploog, Appl. Phys. Lett. **75**, 4019 (1999).
[9] D. Royer and E. Dieulesaint, *Elastic Waves in Solids* (Springer, Heidelberg, 2000).
[10] Y. Takagaki, E. Wiebicke, P. V. Santos, R. Hey, and K. H. Ploog, Semicond. Sci. Technol. **17**, 1008 (2002).
[11] M. Chirita, R. Sooryakumar, R. Venugopal, J. Wan, and M. R. Melloch, Phys. Rev. B **63**, 205301 (2001).
[12] K. Kamitani, M. Grimsditch, J. C. Nipko, C.-K. Loong, M. Okada, and I. Kimura, J. Appl. Phys. **82**, 3152 (1997).
[13] N. F. Naumenko, J. Appl. Phys. **79**, 8936 (1996).
[14] I. S. Didenko, F. S. Hickernell, and N. F. Naumenko, IEEE Trans. Ultrason. Ferroelectr. Freq. Control **47**, 179 (2000).
[15] N. F. Naumenko and I. S. Didenko, Appl. Phys. Lett. **75**, 3029 (1999).
[16] B. A. Auld, *Acoustic Fields and Waves in Solids* (Krieger, Malabar, 1990).
[17] R. R. Reeber and K. Wang, MRS Internet J. Nitride Semicond. Res. **6**, 1 (2001).
[18] M. S. Shur, A. D. Bykhovski, and R. Gaska (unpublished).